Predictive Binder Jet Additive Manufacturing enabled by Clean Burn-off Binder Design

Dustin Gilmer [a, c], Sungjin Kim [b, c], Desarae J Goldsby [b], Peeyush Nandwana[d], Amy Elliott [b*], Tomonori Saito [a, c*]

[a] The Bredesen Center for Interdisciplinary Research and Graduate Education, The University of Tennessee, Knoxville TN 37996, United States
[b] Manufacturing Science Division, Oak Ridge National Laboratory, Oak Ridge, Tennessee 37831, United States
[c] Chemical Sciences Division, Oak Ridge National Laboratory, Oak Ridge, Tennessee 37831, United States
[d] Materials Science and Technology Division, Oak Ridge National Laboratory, Oak Ridge, Tennessee 37831, USA

Corresponding Authors: Amy Elliott, elliottam@ornl.gov

Tomonori Saito, saitot@ornl.gov

Abstract

Binder jet additive manufacturing (BJAM) presents an avenue for advanced manufacturing of various high-value materials due to high deposition rates, scalability, and geometric flexibility. However, conventional organic binders in BJAM introduce residual carbon upon pyrolysis, often leading to imprecise alloy composition in the final sintered part. The undesirable residual carbon from binder burn-off limits the application of BJAM for high-performance alloys due to their high sensitivity to carbon addition. In this study, we have designed poly(vinylpyrrolidone-*co*-vinyl acetate) (PVP-VAc) as a clean burn-off binder for BJAM, where excess oxygen groups in VAc enable cleaner burn-off and reduce residual carbon retention. Compared to a widely used commercial binder, the optimized PVP-VAc binder reduced residual carbon retention by over 90% in H13 tool steel. The significant reduction in residual carbon enables predictable printing and subsequent sintering of complex H13 tool steel geometries, an alloy known to have substantial challenges around distortion due to the sintering window shifting from carbon addition. The design of a clean burnout binder provides a major path forward for BJAM by enabling new AM designs and applications for composition-sensitive high-performance alloys, such as nickel-based superalloys, titanium alloys, and high alloyed steels.

Introduction

Additive Manufacturing (AM) presents technological and industrial promise for its ability to create complex parts from high-value materials that are difficult to form using traditional manufacturing methods. Its lightweight designs with high-value materials using less raw material can boost process efficiencies and reduce greenhouse gas (GHG) emissions [1]. Binder Jet AM (BJAM) represents one of the most promising AM processes for industrial adoption due to its similarity to powder injection moldings in combination with high throughput and low operator burden [2,3]. Many of the advantages of BJAM stem from BJAM's use of inkjet technology [3,4]. In the process, the inkjet printhead selectively deposits a binding fluid (binder) into layers of powder to bind the powder and build up a bound 3D part layer by layer within the powder bed (Fig. 1) [3,5–8] through diverse binding mechanisms. The bound porous composite preform (green part) can be post-processed in various ways, such as sintering to reach full density or higher mechanical strength (Fig.1) [5,8,9]. The binder selection is a critical aspect of the printing process as it can significantly impact the properties of the final part [10]. However, the application of BJAM is currently limited in alloys and geometries due to the adverse effects including structural distortion or compositional alteration caused by the residual binder upon sintering [11]. Therefore, the breakthrough in the manufacturing ecosystem resides in a binder design to mitigate these adverse effects for more efficient high-value alloy materials manufacturing.

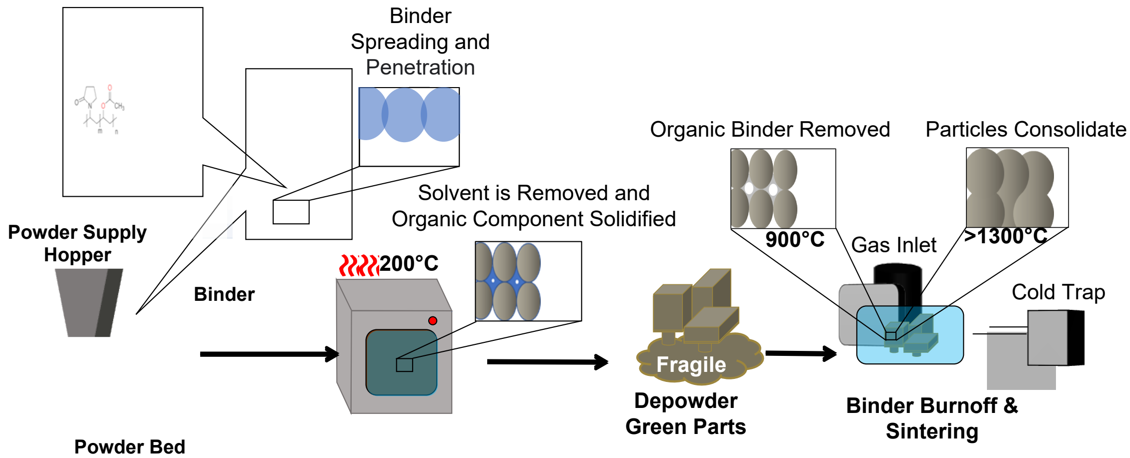

Figure 1: A schematic of the BJAM printing and post-processing: The molecular structure of poly(vinylpyrrolidone-*co*-vinyl acetate) is shown within the binder droplet, with the oxygen molecules in the vinyl acetate repeat unit highlighted in red. After the binder is deposited into the bed in the prescribed geometry, the bed will be cured in an oven to remove the solvent from the binder and solidify the organic portion. The curing, debinding, and sintering temperatures shown in the graphic are representative of H13 for the process flow for this binder and alloy.

Most binders in BJAM utilize an organic component (e.g., monomer, oligomer, or polymer) which solidifies upon heating to bind together the powdered material [12,13]. After the organic binder forms the initial green part, it is typically removed in a debinding process before powder densification (Fig. 1). In BJAM, thermal debinding is the most common method to remove the organic binder portion from the green part [14–16]. During thermal debinding, the organic component undergoes pyrolysis, a series of complex reactions where the organic molecule decomposes into volatile and non-volatile species with lower molecular weight [17,18]. Depending on the debinding temperature, atmosphere, and binder structure, undesirable residual carbon is commonly formed as a non-volatile product during the debinding process [15].

The residual carbon can alter final part properties and distort the final geometries of many high-value alloys as it changes the chemical composition of the alloy [11,19]. A representative example is H13 tool steel, one of the most commonly used alloys for hot and cold working tools, owing to hardenability, strength, toughness, and its high resistance to thermal softening. The use of AM to add features such as cooling channels in these tools and dies could boost process efficiency, reducing the GHG and nitrogen oxide (NOx) emissions associated with downstream manufacturing[1]. One of the most critical adverse effects of residual carbon in H13 tool steels is significant distortion during sintering, caused by the commercial binder leaving behind 0.028-0.07 weight percent (wt%) residual carbon in the H13 alloy [11,20]. This distortion is due to the supersolidus liquid phase sintering (SLPS) temperature of H13 tool steel being sensitive to the amount of carbon. The SLPS temperature can vary significantly with the addition of carbon, often leading to significant distortion in BJAM due to the presence of residual carbon [11]. After sintering, the resulting H13 alloy properties, such as hot working and wear-resistant properties, can be significantly impacted by the alteration in sintering and the addition of excess carbon. Thus, an organic polymer binder that produces less residual carbon is highly desirable for printing H13 tool steel and other alloys.

Minimizing the residual carbon produced by the binder is the key to expanding the printability of carbon-sensitive alloys, such as H13, which are conventionally challenging to achieve precise printed structures. In the following work, a clean burn-off binder is designed that consists of poly(vinylpyrrolidone-*co*-vinyl acetate) (PVP-VAc), a copolymer of poly(vinylpyrrolidone) (PVP), and poly(vinyl acetate) (PVAc). PVAc releases oxygen during polymer decomposition, which is expected to react with residual carbon from PVP to produce more volatile components to reduce the residual carbon left behind after thermal debinding (Fig.1)[21–23]. Unraveling how the alteration of the binder molecule affects carbon retention is crucial to controlling residual carbon and expanding the range of high-performance materials used in BJAM to form high-fidelity structures for industrial tooling and power generation components [10,24]. The design of a clean burnout binder (PVP-VAc) to mitigate the adverse effects of the binder on sintering provides a pathway for the predictable formation of various high-value alloy materials such as nickel-based superalloys, titanium alloys, and high alloyed steels.

2. Experimental

2.1 Materials

The study used gas-atomized H13 powder procured from Sandvik Osprey Ltd, and the powder was identical to the powder used in Nandwana et al.'s study on the microstructural evolution of BJAM H13, which has a *d10* of 13.68 µm, a *d50* of 19.72 µm, and a *d90* of 32.03 µm, respectively[11]. The 1-vinyl-2-pyrrolidinone (VP) and vinyl acetate (VAc) monomers were obtained from Sigma Aldrich and run through a column to remove the inhibitor before polymerization. 2,2-azobisisobutyronitrile (AIBN) from Sigma Aldrich was recrystallized from methanol. Ethanol, diethyl ether, 1-propanol (ACS grade, 99.5+%), and deionized water (H_2O) were obtained from Sigma Aldrich and used as received. Iso-propanol (70%) was obtained from McMaster-Carr and used as received. Commercial Poly(vinylpyrrolidone-co-vinyl acetate) (PVP-VAc) (W-635) was obtained from Ashland, which had a number average molecular weight (M_n) of 13,000 g/mol.

2.2 Synthetic Method for Poly (1-vinylpyrrolidone-co-vinyl acetate)

The synthesis of PVP-VAc was adapted from Thang et al. [25]. A free radical polymerization method was utilized in which AIBN was used as the free radical initiator. 1.806 g of the AIBN initiator, 1.8wt% compared to the monomer mixture was added to a 2L round bottom flask containing 53.7 mL of VP, 47.1 mL VAc and 1,458 mL of ethanol. The solution was sealed and purged with nitrogen to remove oxygen for five minutes and then placed into a temperature-controlled oil bath at 65 °C. The solution was kept stirring at 65 °C for 18 hours. After 18 hour-reaction, the reaction mixture was purified, and any excess monomer was removed by precipitating the solution into diethyl ether. The solid polymer was separated from the residual monomer or unreacted initiator using a centrifuge. The excess solvent was evaporated from the polymer, and the isolated yield of PVP-VAc reached 88.9 %. The structure was confirmed using ^{1}H NMR spectroscopy using a Bruker Avance III 400Hz.

2.3 Binder preparation

Two different PVP-VAc binder solutions were prepared. The first binder solution was prepared using commercial PVP-VAc (W-635), and the polymer (5 wt%) was mixed into a solution of 80/20 = H_2O/1-Propanol. The second binder solution was by mixing the synthesized PVP-VAc into a solution at 10 wt% with the remaining 90 wt% consisting of a mixture of 80/20 Water (H_2O) (80 wt%)/1-Propanol (20 wt%).

2.4 Binder Jetting

An Innovent binder jet printer from ExOne Corporation was utilized for printing 3-point bend specimens. ExOne Corporation provided their aqueous binder AquaFuse. Three samples were tested at 85 %, 100 %, and 105 % saturation for the low molecular weight (MW) synthesized PVP-VAc formulated binder and the Aquafuse binder. The printer was equipped with a printhead containing four SL-128 AA modules from Fuji Films. This configuration creates 80 pL droplets and has 128 nozzles with a 50 µm diameter nozzle size. To dispense powder the ExOne Innovent that was utilized in this research was equipped with the pneumatic vibratory manifold with an additional oscillating foot to assist with the dispensing of powders

A new binder is introduced to the Innovent system in an identical fashion that it would be introduced to an X1-Lab binder jet printer, which is described in Gilmer et al.[23]. Heat is used during printing as well to remove solvent from the mixture. The operation of the heater is described in Dvorak et al.[21]. During printing, saturation is used to determine the amount of binder that is deposited within the powder bed. A description of saturation can be found in Gilmer et al.[22]. Values utilized to print the specimens tested are listed below (Table 1).

Table 1 Printing parameters for 3-point bend specimen

Parameters	85 % Saturation	100 % Saturation	105 % Saturation
Layer Thickness (µm)	25	25	25
Y Droplet Spacing (µm)	67.2	76.2	72.5
X Droplet Spacing (µm)	84.7	63.5	63.5
Powder Packing Rate (%)	60	60	60
Last Drop Volume ($\boldsymbol{pL}$)	48.4	48.4	48.4
Dry Time Between Layers (sec)	3.5	10	10
Roller Speed (RPM)	225	250	250
Roller Speed (mm/s)	10	10	10

After printing, the entire powder bed is placed into the curing oven as described in Gilmer et al.[25]. The same parameters were utilized for curing the synthesized PVP-VAc binder that is utilized with the commercial binder (200°C for 2 hours) to ensure no confounding variables were introduced.

2.5 Sintering and Debinding Parameters

Sintering parameters for the printed parts using synthesized PVP-VAc binder were developed based on previous work by Nandwana et al., where the samples were heated at a ramp rate of 10 °C/min to 900 °C and held for three hours to allow for binder burnout and debinding [11].

The samples were sintered at 1360, 1380, and 1400 °C at a ramp rate of 10 °C/min and held for five hours for densification. The binder burnout and sintering were conducted in a single step in a vacuum furnace equipped with graphite heating elements under a vacuum of 10^{-5} mTorr. The samples were allowed to undergo furnace cooling at the end of the cycle, and the average cooling rate was recorded to be ~4−7 °C/hour.

2.6 Characterization

2.6.1 Binder Characterization

The viscosity of the binders was measured by Electromagnetically Spinning Viscometer (EMS) utilizing an EMS-1000 from Kyoto Electronics Manufacturing Co. [22,26].

2.6.2 Mechanical Characterization

Mechanical testing of the green parts was performed using a custom-made three-point bend instrument and were tested according to the protocol established in Gilmer et al.'s previous work on custom binder formulation [22].

2.6.3 Chemical Characterization

Chemical analysis on the powders and the samples was conducted for carbon using combustion infrared detection per ASTM E1019-18. ^{1}H NMR spectra were recorded on a Bruker instrument (400 MHz) and internally referenced to the residual solvent signals of $CDCl_3$ for ^{1}H at 7.26 ppm. A dimethylformamide gel permeation chromatography unit was used and further description of the instrument can be found in Jacobs and Brantley [27].

2.6.4 Thermal Characterization

The coupling of the Thermogravimetric Analysis (TGA) (TA Instruments, Discovery model 5500) with a Cirrus 3 MKS mass spectrometer (MS) made it possible to identify the MS fractions of the evolved gas during thermal degradation of synthesized and commercial PVP-VAc binders. The TGA was completed by ASTM E1131, ISO 11358 at a ramp rate of 10 °C/min in Argon atmosphere. During decomposition, the gaseous species were introduced into the Cirrus 3 MKS mass spectrometer (MS) via a heated (300 °C) stainless-steel capillary to the MS inlet orifice. The samples were then ionized and passed through a mass filter to the detector, where the ionized gas was sorted by its mass charge ratio, and the ion current was measured.

2.6.5 Structural Characterization

X-Ray Computed Tomography (XCT) measurements were performed using a Zeiss Metrotom 800HR 225 kV XCT instrument. A .25mm copper filter was used during the scans, which were performed at 180 kV at 55 mA. A 1000mS integration time was used for the images, which were averages across two images. The scan image/voxel resolution was 7.08mm. XCT using these parameters was performed on two samples printed at different saturations and sintered using the same parameters to show the difference in densification due to the residual carbon amounts. Data acquisition and reconstruction with the XCT setup were performed using the Zeiss Scout and Scan software v.11. VG Studio Max 3.4 was used for the data analysis, with VG easy pore module for pore analysis. The thresholding used in this software specifically bases the pore analysis on contrast in the XCT image

3. Results and Discussion

When the design of PVP-VAc binder was considered for the BJAM system, the commercially available PVP-VAc polymers was initially evaluated. However, they present a significant challenge to be used in inkjet deposition systems due to their inherent high viscosities. The high viscosity of the binder solutions with commercial PVP-VAc (W-635) necessitates low polymer loading in the binder formulations, as any viscosity greater than 20 mPa*s is not printable in the current inkjet systems (Fig.2a). Attempts were made to print with these lower solid loading binders with the correct viscosity range, but parts printed using these low solids loading binders (e.g. 2.5 or 5.0 wt%) were fragile and did not survive the depowdering processes (Fig.2b). In BJAM, lower solids loading often leads to lower green strengths in the green parts, which leads to breakage during the depowdering of the green parts [28,29].

a

concentration (wt%)	viscosity (mPa*s)
2.5	11.5
5	13.6
7.5	17.4
10	21.6
12.5	26.3
15	35.3

b

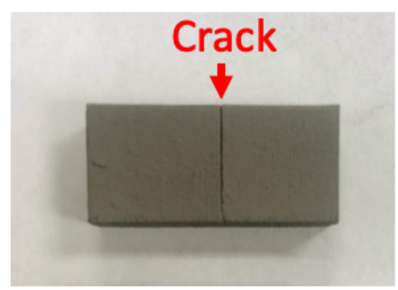

Figure 2. a)Viscosity as a function of the weight percent (wt%) of the commercial PVP-VAc in the solution b)Image of broken bar formed using low-concentration binder

In part, the MW of the polymer dictates the viscosity of the formulations [30]. Therefore, a lower MW polymer is needed to formulate a binder solution with a higher loading of PVP-VAc polymer and increase the green strength to form viable green parts. Thus, a lower MW PVP-VAc polymer was synthesized to increase the polymer loading and improve the green strength of a PVP-VAc binder.

3.1 Synthesis and Structural Characterization of Low Molecular Weight PVP-VA

The lower MW PVP-VAc copolymers were prepared through free-radical copolymerization in a solution of ethanol, using AIBN as the free radical initiator (Fig.3). The reaction at high concentration and short reaction time generally produces higher MWs with reduced yield, which leads to higher viscosity solutions, and makes them unsuitable for binder solution in this application [31]. To synthesize low MW PVP-VAc, a highly diluted solution (8 wt% monomer in 92 wt% ethanol) as well as high concentration of AIBN was used in combination with a long reaction time (18 hours) for achieving high yield. The reaction condition produced a low M_n of 8,600 g/mol and a polydispersity index of 2.21, which was determined using DMF GPC. In comparison, when a higher concentration was used for the polymerization at approximately 50 wt% monomer and 50 wt% solvents, the resulting number average molecular weight (M_n) was much greater in the range of 60,000 g/mol. The lower M_n compared to that of 13,000 g/mol for the commercial PVP-VAc enables jettable binder solution at higher concentration. The conversion to PVP-VAc was calculated using Eq.3, where H is the conversion of monomer (%), m is the product weight (g), and m_o is the initially charged monomer weight (g). The reaction yielded 88.9 % conversion to polymer from the starting material.

$$H = \frac{m}{m_0} \times 100 \tag{3}$$

The ratio of VAc/VP is critical due to insolubility of VAc and solubility of VP in polar solvents such as water. If the ratio of VA in the polymer is too high, it will not be able to be utilized in aqueous binder systems, which is the most common system utilized in BJAM. The ratio of VP to VAc in the polymer was determined using ^{1}H NMR and determined to be 33% VP to 77% VAc as a random copolymer. The ratio of 33% VP to 77% VAc remained soluble in water, making it ideal for utilization in an aqueous BJAM binder system.

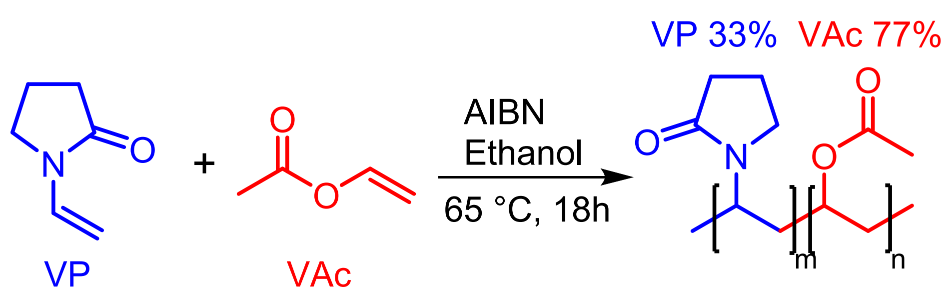

Figure 3: Free radical polymerization yielding PVP-VAc

3.2 Binder formulation

Once the polymer is synthesized, it must be formulated into a binder. Binders in a drop-on-demand system must have specific rheological characteristics to eject from the printhead orifice and form a stable droplet. The Z parameter (Z = 1/Oh) (Eq. 4) is often used to determine the printability of a fluid from an inkjet printhead, where Oh is the Ohnesorge number (Eq. 5), a combination of the rheological characteristics of the ink.

$$Z\ number = \frac{1}{Oh} \tag{4}$$

$$Oh = \frac{\mu}{\sqrt{\gamma \rho L}} \quad (5)$$

Reis and Derby used numerical simulations and proposed a Z range from 10 > Z > 1 for stable droplet formation [32]. This range of Z numbers places the jettable solution viscosities from 1-20 mPa*s and surface tensions from 20-40 mN*m^{-1}, with these two properties having the most significant effect on the printability of the binder [28,29]. When the Z < 1 corresponds to a lower Reynolds number, the fluid has a high viscosity. The high viscosity will cause viscous dissipation in the liquid, when the piezoelectric element expands, preventing the liquid from ejecting from the printhead [33]. Conversely, if a binder has a Z > 10, this corresponds to low viscosities and formation of satellite droplets upon ejection, which will cause inconsistent binder deposition and lower print accuracies [32,34–36].

Binders utilize a mixture of a polymer with solvent to provide the rheological characteristics necessary for printing in an inkjet system. When formulating the binder, two types of solvent systems can be utilized in BJAM: aqueous or non-aqueous. Aqueous systems are the most common since they present a safer approach than non-aqueous systems that often utilize flammable or hazardous solvents. Aqueous systems use water as the primary solvent in the system but, in most cases, have additives incorporated to increase the wettability, decrease surface tension, or reduce the drying rate [37–39]. Several surfactants can be added to an aqueous solution to achieve the desired decrease in surface tension, such as ethanol, methanol, butanol, propanol, and isopropanol. 1-propanol was chosen in this work due to its compatibility with PVP-VAc and lower vapor pressure than other organic solvents. The synthesized low MW PVP-VAc in water/1-propanol mixture provided a range of possible formulations suitable for printing (Table 2). 10-20 wt% of PVP-VAc in water/1-propanol = 80/20 solution gave Z numbers ranging between 2.54-5.89, calculated using the rheological properties of the fluid.

Table 2. Parameters and properties (loading, density, viscosity, surface tension, nozzle radius) used for calculating the Z and Ohnesorge numbers equations four and five.

PVP-VA Loading (wt%)	Density (ρ) (g/mL)	Viscosity (μ) (mPa.s)	Surface Tension (γ) (mN/M)	Nozzle Radius (L) (µm)	Ohnesorge Number (Oh)	Z number
10	1.01	5.05	35	25	0.17	5.89
15	1.01	7.94	35	25	0.27	3.74
20	1.01	11.7	35	25	0.39	2.54

As their Z numbers fall between 1-10, all these formulations can form stable droplets that are printable in the Innovent printer. We down-selected a formulation with lower viscosity and higher Z number due to those parameters known to form stronger green parts [23,40]. Thus, the 10 wt% solids loading was down-selected for printing in the remainder of the experiments.

3.3 Green Part mechanical properties

The strength of the green part is one of the most critical properties in BJAM, as the green strength determines if the part will survive the depowdering stage without failure or distortion. If the green part breaks during the depowdering process, the part's geometry will no longer match the designed final part geometry. There is an established positive correlation between the volume of binder within a green part defined by the saturation/wt% of binder in the part and the flexural strength of the part from this work and previous work [22,23,41]. Thus, it is essential to consider saturation when determining the strength of the green parts (Fig. 4). For this work, green parts of H13 steel tool were fabricated utilizing the synthesized PVP-VAc binder with a 10 wt% solids loading. The results shown in Figure 4 show that the green strength increased linearly with the increase of binder saturation/ amount of polymer within the sample.

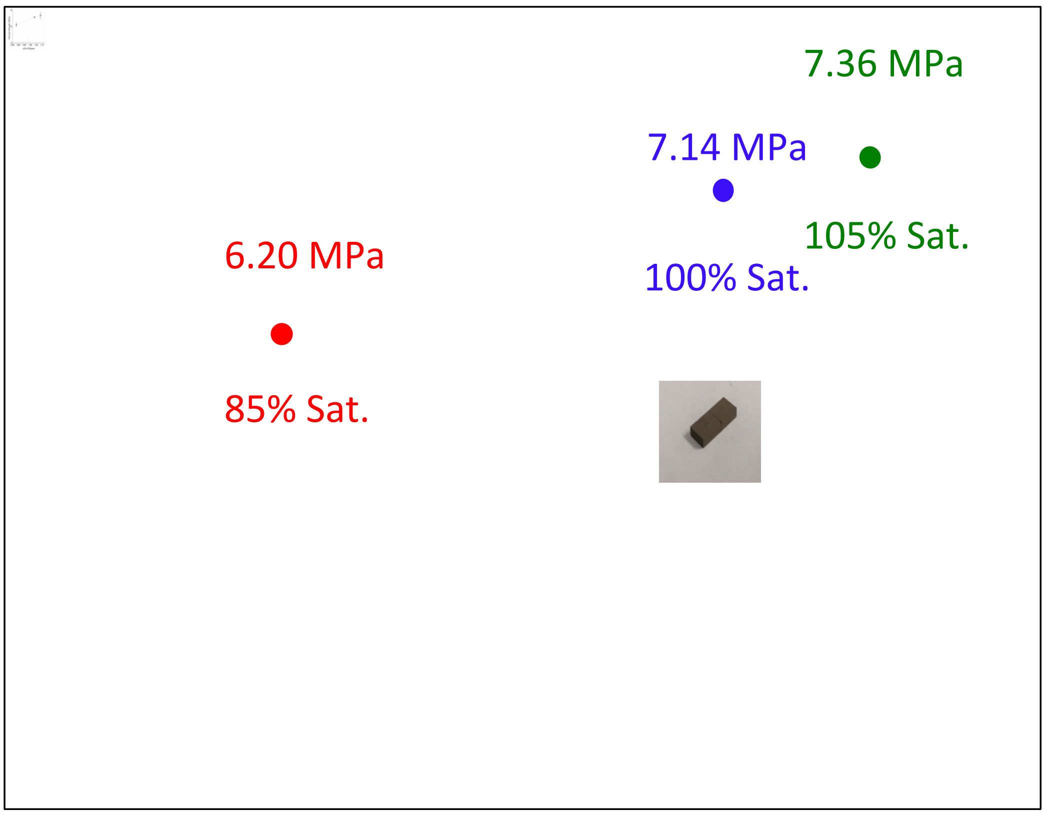

Figure 4: Flexural strength of the synthesized PVP-VAc binder at saturations of 85%,100%, and 105% with H13 steel particles.

At an 85 % saturation (0.88 wt% in the printed H13 part), the flexural strength of the green parts exhibits 6.20 MPa, comparable to the commercial binder at the same saturation with stainless steel 420, 6.65 MPa [22]. Since stainless steel 420 is one of the most commonly utilized alloys in BJAM and this green strength is commonly used for handling of parts, it is expected that this green strength should be sufficient for depowdering and handling of green H13 parts formed with the PVAc binder. Upon depowdering of the printed samples, all of the parts printed with PVP-VAc survived depowdering, supporting this expectation. The flexural strength can be further improved at higher saturation, reaching 7.14 MPa and 7.36 MPa at 100% saturation (1.04 wt% in the printed H13 part) and 105% saturation (1.07 wt% in the printed H13 part), respectively. As discussed in the previous section, one of the major observations from the various binder formulations tested is that higher Z number fluids with a lower viscosity show a trend of having a higher green strength from this work and prior work by Gilmer et al. [22,23]. It is assumed this is due to the fluid being able to incorporate better into the powder bed, but it is difficult to decouple the impact of fluid properties from other factors, such as polymer loading.

3.4 Binder Thermal Debind and pyrolysis

The binder burnout and pyrolysis of the organic component in the BJAM process is a complex chemical and physical process that has garnered minimal attention. Most studies centered around thermal debinding have focused on aspects of the debinding process, such as the ramp rate, hold time, and hold temperature. Some aspects of the chemical processes at these temperatures have been explored by varying the burnout atmospheres. However, no studies in BJAM to date have considered the organic molecule used for binding or attempted to manipulate the molecule to alter the debinding behavior of the part.

Polymer removal by thermal debinding involves the thermal degradation or pyrolysis of the polymer into volatile gas species and non-volatile solids such as residual carbon [15]. Pyrolysis is a complex reaction but can be simplified by considering thermal degradation as a free radical process [42]. The dissociation of bonds is caused by thermal energy and produces free radicals. Thus, the dissociation mechanism can be considered a free radical degradation based on the types of chemical bonds involved and the stability of the small molecules produced during the degradation [42]. In the free radical degradation mechanism, the weakest bond will break first. In the case of simple carbon-carbon bonds, the molecule with the lower number of bonds is the strongest. This means that the bonds will break in the order of 3° > 2° > 1° > CH_3 [42]. After the bonds break, intramolecular rearrangements will produce more stable free radicals. The type of polymer and bonds are thus important for how the polymer will degrade. If the polymer consists of a simple carbon backbone, such as polyethylene, random scission between the bonds is known to take place where the chain will break down into a distribution of smaller molecules. However, a common degradation mechanism for copolymers is scission between the two copolymer units, thus reverting the chain into its monomeric form [42,43].

This PVP-VAc copolymer's degradation mechanism of bond-breaking between the constituent monomers can be observed by comparing the pyrolysis behavior of the individual polymers and the copolymer system. The burnout behavior of VP and VAc unit is shown by the pyrolysis behavior of PVP and PVAc homopolymers observed by TGA (Fig.5). Due to the higher stability of the bonds in the PVP molecule, it does not degrade until a higher temperature than PVAc, which begins to degrade before 400°C [44–46].

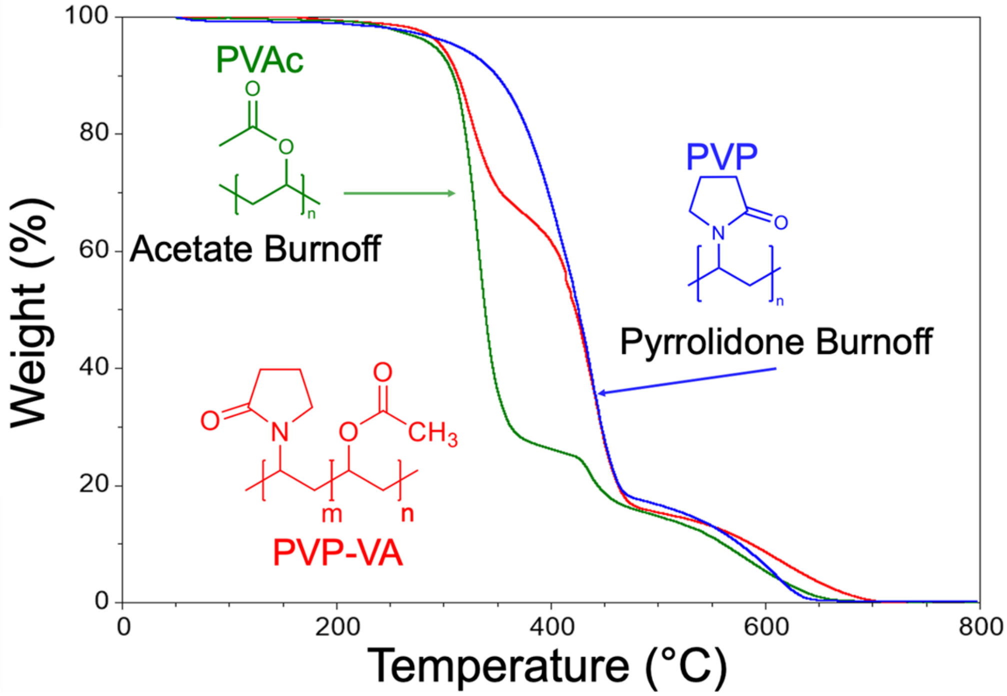

Figure 5: TGA curve showing the degradation of PVP, PVAc, and PVP-VAc. The curves illustrate the varying degradation temperatures of the constituent molecules in the PVP-VAc copolymer showing how the polymer breaks down into its constituent polymers.

Due to the breakdown of the PVAc structure in the copolymer at lower temperatures, more oxygen (O_2) is available from the acetate monomer to form gases such as carbon dioxide (CO_2) and/or carbon monoxide (CO) during binder burnout. The excess O_2 should reduce the solid residual carbon as more carbon can escape as a volatile gas. TGA-MS data confirm that one of the significant degradation products is O_2 during PVAc pyrolysis (Fig.6a). In contrast, when PVP undergoes degradation, O_2 production from the polymer degradation is minimal compared with that of the PVAc degradation (Fig.6b). This reduced O_2 generation reduces the subsequent CO_2 formation (Fig.6b).

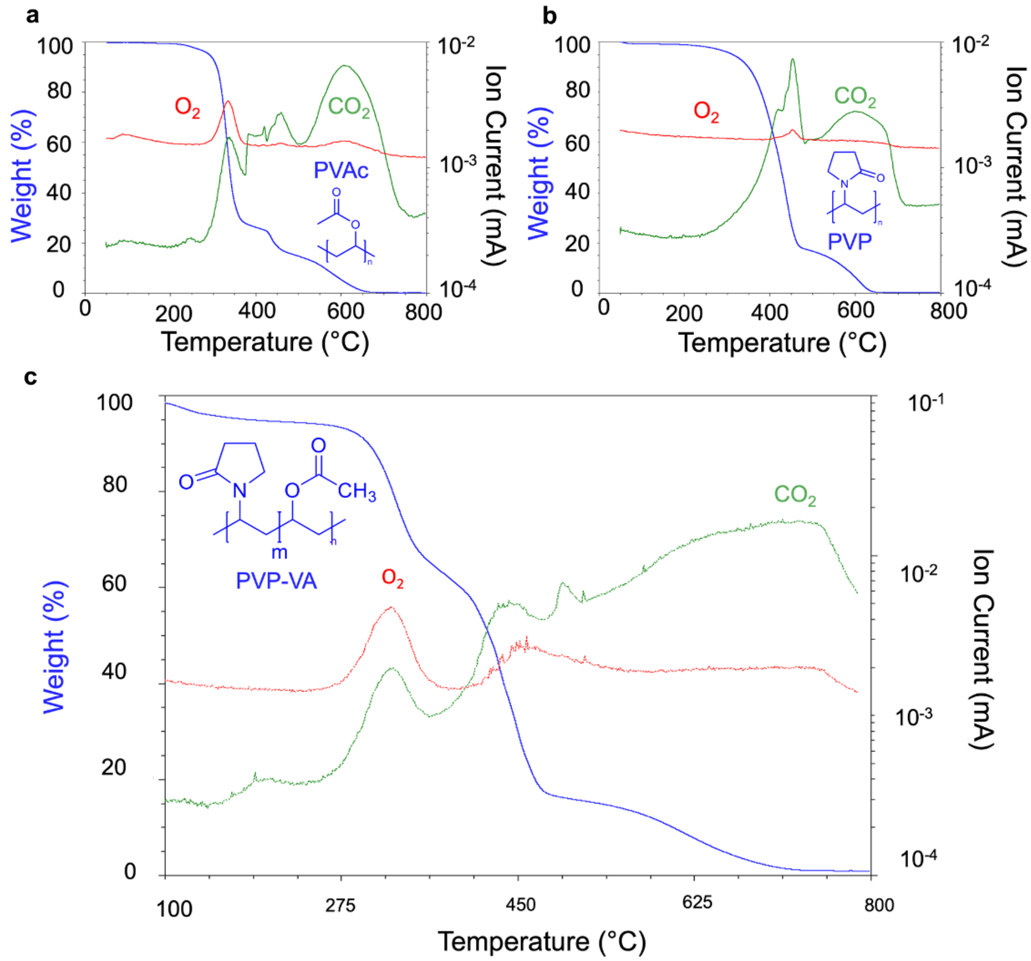

Figure 6: a) TGA-MS showing the degradation of PVAc and the O_2 and CO_2 produced because of the degradation. b) TGA-MS showing the degradation of PVP and the O_2 and CO_2 that is produced because of the degradation. c) TGA-MS showing the degradation of PVP-VAc and the O_2 and CO_2 produced by the polymer degradation.

When PVP-VAc undergoes degradation, O_2 is one of the major early degradation products due to the breakdown of the polymer chain into its monomer components and the degradation of the PVAc portion (Fig.6c). Furthermore, the continued presence of CO_2 after the degradation of the PVAc portion, as shown by the MS fraction, corroborates that the excess O_2 from PVAc increases the formation of volatiles during polymer degradation. This excess O_2 should generate more CO_2 intensity in the MS and would result in a binder with less residual carbon than the commercial binder after the debinding process.

3.5 Sintering & Chemical Characterization

The cubed-shaped printed parts were heated at 10 °C/min to 900 °C and held isothermally for 3 hours for debinding cycle, followed by ramping up at 10 °C/min to the final sintering temperatures of 1360, 1380, and 1400 °C for 5-hour sintering process. The impact of PVP-VAc burn-out behavior on the reduction in residual carbon was systematically investigated using combustion analysis to quantify the residual carbon amounts (Table 3). To compare with current binders utilized in BJAM, the residual carbon values for the PVP-VAc binder were benchmarked against the residual carbon produced by the commercial Aquafuse after binder burnout and sintering, as the commercial binder has been shown to produce levels of residual carbon that negatively affect the shape retention and properties of many alloys [11]. When compared with the commercial Aquafuse binder, the use of PVP-VAc binder printed and pyrolyzed at similar conditions resulted in a reduction of residual carbon retention by over 90% in the combustion analysis results (Table 3) when used with H13 tool steel. Such reduction of residual carbon in the other alloys is expected, while the exact degree of residual carbon reduction would depend on the type of alloy.

To understand how the PVP-VAc binder produces less residual carbon, we conducted the TGA-MS (Fig. 6) to analyze the molecules produced during the debinding process. The TGA-MS of the PVP-VAc polymer during heating indicates that the PVP-VAc polymer produces CO_2 after the degradation of the oxygen-containing portion of the polymer. The carbon susceptible for oxidation produces this CO_2 during the polymer degradation, as this would remove carbon atoms as a gas phase instead of leaving them behind as a solid char. The combustion analysis (Table 3) indicates the reduction in residual carbon upon pyrolysis of PVP-VAc compared to other polymer systems that do not contain oxygen in the polymers. The strategy to reduce residual carbon utilizing PVP-VAc binder eliminates the carbon contamination issue for many alloys, such as H13, and makes it possible to find predictive sintering windows by not altering the chemical composition (Fig.7).

Table 3. Carbon content in sintered H13 parts with commercial binder and varying saturations (Sat) and sintering temperatures (Carbon content (%) data from commercial binder was reproduced from [11]) the standard deviation for the residual carbon values is 0.00122%. The percentage of carbon reduction was calculated by the following formula [(Commercial binder carbon content – PVP-VAc binder carbon content) / Commercial binder carbon content] × 100]

Binder	Binder Content (wt%)	Carbon Content (%) Commercial Binder	Carbon Content (%) PVP-VAc Binder	Carbon Reduction (%) from Commercial Binder to PVP-VAc
85% Sat 1360°C	0.88	0.541	0.135	75.04
105% Sat 1360°C	1.09	0.557	0.135	75.76
85% Sat 1380°C	0.88	0.363	0.073	79.88
105% Sat 1380°C	1.09	0.406	0.064	84.23
85% Sat 1400°C	0.88	0.456	0.013	97.14
105% Sat 1400°C	1.09	0.499	0.030	91.13

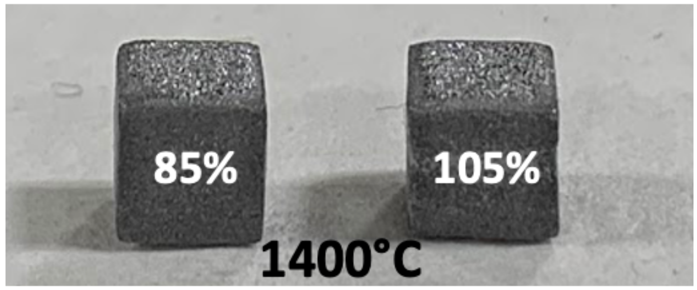

Figure 7: Image of two H-13 samples, one printed with 85% saturation and the other printed at 105% saturation. Both samples were sintered at 1400°C and showed minimal distortion at high binder saturations.

To evaluate the sintering mechanism and how the chemistry of the sample affected the sintering process, the final densities and porosities of a sample printed with the PVP-Vac binder were compared to a sample printed with the commercial binder. To quantify the porosity/density of the sintered samples, X-ray Computed Tomography (X-CT) was utilized. The 85% saturation sample has a density of approximately 96%, while the 105% saturation sample has a sintered density of approximately 95% after sintering at an ultimate temperature of 1400°C following the parameters discussed in section 2.5. The porosity can be seen from the X-CT image, which is comprised of small pores in the sample dispersed throughout the part with no large pores being present (Fig. 8). These final densities are slightly lower than those of the same saturation that were measured by Nandwana et al. [11]. This could be for various reasons, but one of the reasons is likely because the samples did not enter into the liquid sintering regime that the samples in Nandwana et al.'s work experienced due to the reduction in carbon content. Other reasons include the difference in density measurement techniques, Archimedes vs. XCT, as well as variations in green density.

In addition to porosity measurements, the distortion was measured by using calipers to measure the X, Y, and Z dimensions of the samples, and calculating the percent (%) difference between the printed and sintered samples. In each sample, the percentage of distortion was calculated to be below 10% from the printed to the sintered samples, and the majority of samples had distortion in the single digits. For the samples shown in Figure 7, the distortion for the sample printed with the PVP-VAc binder at 85% saturation was 4% in the Y direction, 3% in the X direction, and 2% in the Z direction, and the 105% saturation prints had a distortion of 1% in the Y direction, 5% in the X direction, and 5% in the Z direction. The degree of distortion in this study was considered minimal compared to the major distortion seen in the samples from Nandwana et al.'s work, where the samples were distorted due to entering the liquid sintering phase because of excess residual carbon[11].

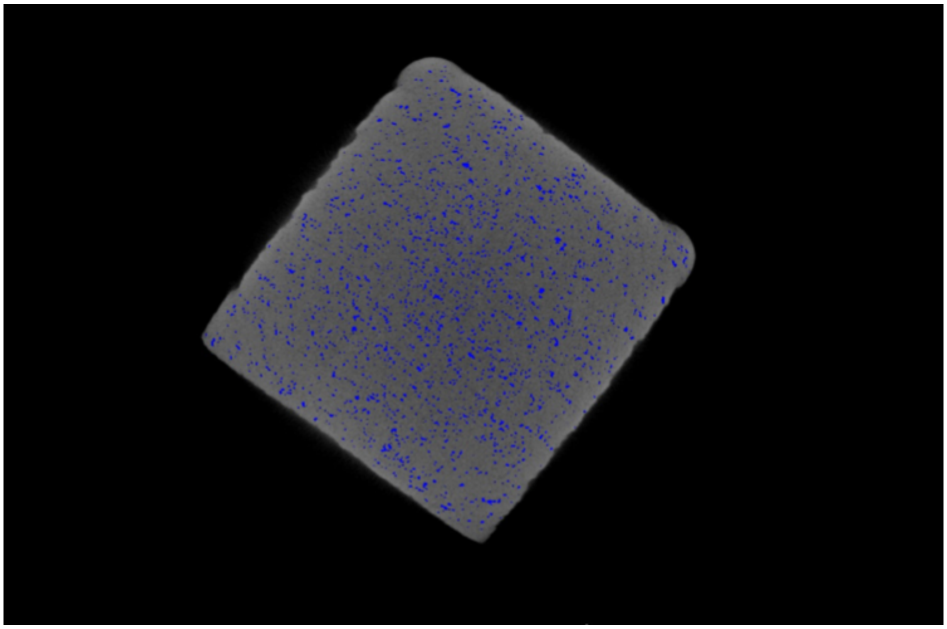

Figure 8: Image capture of the X-ray Computed Tomographic scan performed on the PVP-VAc 105% saturation H13 cube sintered at 1400°C. The blue in the image represents void space within the part, while the gray represents solid material.

4. Conclusion

We have presented a simple binder design consisting of PVP-VAc polymer that dramatically reduces residual carbon production. High MW of commercially available PVP-VAc was tested but limited the solids loading of the binder due to its high viscosity, which led to poor mechanical green strength in the green parts. Thus, a lower MW PVP-VAc was synthesized to accommodate a higher loading of 10 wt% and maintain a suitable viscosity of 5.05 mPa*s for ink jetting. This higher solid loading of PVP-VAc in the binder enables the formation of parts with a green strength equivalent to that of the commercial binder, adequate for depowdering and handling. The two-step degradation of PVP-VAc reduces residual carbon retention by greater than 95% compared to the commercial ExOne Aquafuse binder. The release of O_2 during the degradation of the PVAc portion in the polymer facilitates CO_2 formation and diverts the residual carbon formation during PVP degradation. The PVP-VAc binder will help create a more predictable binder decomposition during the debinding process and reduce the residual carbon formation, which results in reduced distortion during SLPS sintering. The clean burnout PVP-VAc binder expands the range of printable high-performance alloys like H13 steel, which have been thus far challenging to print accurately due to distortion. Specifically, when H13 steel was printed with 105% saturation of PVP-VAc binder, the green strength reached 7.36 MPa, and subsequent sintering at 1400°C resulted in a 91% reduction in carbon content compared to the current commercial binder. This reduction in residual carbon formation during the sintering of H13 steel lowers the overall carbon levels of the alloy to keep it within the expected range. This results in the alloys' sintering process being predictable, and thus prevents liquid formation in the component during sintering, which can often result in the deformation of the component. Beyond H-13 tool steels, this clean burnout binder or similar analogs will enable the printing of other alloys, such as Ni, Al, or Ti alloys, all of which are sensitive to residual carbon during the forming process. Unlocking the ability to print these high-performance alloys using low-carbon binders in BJAM will present a new opportunity to deliver high-complexity parts that previously were difficult to form from these alloys. Furthermore, the O_2/CO_2-generating binder design can be utilized not only in BJAM but also in other powder metallurgy applications to reduce the residual carbon, which can broadly impact materials manufacturing and processing technologies.

Acknowledgments

The research was sponsored by the U.S. Department of Energy, Office of Energy Efficiency and Renewable Energy, Advanced Materials and Manufacturing Office. The author is grateful for a fellowship from the Bredesen Center for Interdisciplinary Graduate Education. The author would also like to thank Mr. Andres Marquez for his assistance with the X-CT portion of the manuscript.

References

[1] P. Nandwana, R. Kannan, D.N. Leonard, Leveraging Solute Segregation in Laser Powder Bed Fusion to Achieve Superior Strength and Ductility Via Single-Step Heat Treatment in Ti-Free Grade 300 Maraging Steel, JOM. 72 (2020) 4221–4231. https://doi.org/10.1007/s11837-020-04435-7.

[2] A. Hosny, S.J. Keating, J.D. Dilley, B. Ripley, T. Kelil, S. Pieper, D. Kolb, C. Bader, A.M. Pobloth, M. Griffin, R. Nezafat, G. Duda, E.A. Chiocca, J.R. Stone, J.S. Michaelson, M.N. Dean, N. Oxman, J.C. Weaver, From improved diagnostics to presurgical planning: High-resolution functionally graded multimaterial 3D printing of biomedical tomographic data sets, 3D Print Addit Manuf. 5 (2018) 103–113. https://doi.org/10.1089/3dp.2017.0140.

[3] A.M. Elliott, L.J. Love, Operator burden in metal additive manufacturing, in: Solid Freeform Fabrication 2016: Proceedings of the 27th Annual International Solid Freeform Fabrication Symposium - An Additive Manufacturing Conference, SFF 2016, 2016: pp. 1890–1899. http://energy.gov/downloads/doe-public-.

[4] J.A. Gonzalez, Characterization and Comparison of Metallic and Ceramic Parts Fabricated Using Powder Bed-Based Additive Manufacturing Technologies, (2017) 142.

[5] E. Sachs, M. Cima, J. Cornie, J. Bredt, A. Fan, K. Lee, B. Pruitt, P. Williams, Dimensional Printing: Rapid Tooling and Prototypes Directly from CAD Representation, Solid Freeform Fabrication Symposium. (1990) 27–47. https://doi.org/10.1016/S0007-8506(07)61035-X.

[6] J.A. Gonzalez, Characterization and Comparison of Metallic and Ceramic Parts Fabricated Using Powder Bed-Based Additive Manufacturing Technologies, (2017) 142.

[7] E. Sachs, M. Cima, P. Williams, D. Brancazio, J. Cornie, Three dimensional printing: Rapid tooling and prototypes directly from a CAD model, Journal of Manufacturing Science and Engineering, Transactions of the ASME. 114 (1992) 481–488. https://doi.org/10.1115/1.2900701.

[8] T. Method-, Standard Terminology for Additive Manufacturing – General Principles –, i (2017) 1–9.

[9] Z.C. Cordero, D.H. Siddel, W.H. Peter, A.M. Elliott, Strengthening of ferrous binder jet 3D printed components through bronze infiltration, Addit Manuf. (2017). https://doi.org/10.1016/j.addma.2017.03.011.

[10] P. Nandwana, A.M. Elliott, D. Siddel, A. Merriman, W.H. Peter, S.S. Babu, Powder bed binder jet 3D printing of Inconel 718: Densification, microstructural evolution and challenges☆, Curr Opin Solid State Mater Sci. 21 (2017) 207–218. https://doi.org/10.1016/j.cossms.2016.12.002.

[11] P. Nandwana, R. Kannan, D. Siddel, Microstructure evolution during binder jet additive manufacturing of H13 tool steel, Addit Manuf. 36 (2020) 101534. https://doi.org/10.1016/j.addma.2020.101534.

[12] M. Ziaee, N.B. Crane, Binder jetting: A review of process, materials, and methods, Addit Manuf. 28 (2019) 781–801. https://doi.org/10.1016/j.addma.2019.05.031.

[13] F.K. Feenstra, Method For Making a Dental Implant, US 6,955,776 B1, 2005. https://doi.org/10.1016/j.(73).

[14] A. Mostafaei, A.M. Elliott, J.E. Barnes, C.L. Cramer, P. Nandwana, M. Chmielus, Binder jet 3D printing – process parameters, materials, properties, and challenges, Prog Mater Sci. (2020) 100684. https://doi.org/10.1016/j.pmatsci.2020.100684.

[15] R.K. Enneti, S.J. Park, R.M. German, S. V. Atre, Review: Thermal debinding process in particulate materials processing, Materials and Manufacturing Processes. 27 (2012) 103–118. https://doi.org/10.1080/10426914.2011.560233.

[16] K.S. Hwang, H.K. Lin, S.C. Lee, Thermal, solvent, and vacuum debinding mechanisms of PIM compacts, Materials and Manufacturing Processes. 12 (1997) 593–608. https://doi.org/10.1080/10426919708935169.

[17] G. Aggarwal, S.J. Park, I. Smid, R.M. German, Master decomposition curve for binders used in powder injection molding, Metall Mater Trans A Phys Metall Mater Sci. 38 (2007) 606–614. https://doi.org/10.1007/s11661-007-9102-0.
[18] E. Apaydin-varol, S. Polat, A.E. Putun, PYROLYSIS KINETICS AND THERMAL DECOMPOSITION BEHAVIOR OF POLYCARBONATE – a TGA-FTIR study, 18 (2014) 833–842. https://doi.org/10.2298/TSCI1403833A.
[19] A. Mostafaei, J. Toman, E.L. Stevens, E.T. Hughes, Y.L. Krimer, M. Chmielus, Microstructural evolution and mechanical properties of differently heat-treated binder jet printed samples from gas- and water-atomized alloy 625 powders, Acta Mater. (2017). https://doi.org/10.1016/j.actamat.2016.11.021.
[20] R. Kannan, P. Nandwana, Predicting sintering window during supersolidus liquid phase sintering of steels using feedstock analysis and CALPHAD, Mater Lett. 304 (2021) 1–9. https://doi.org/10.1016/j.matlet.2021.130648.
[21] J. Dvorak, D. Gilmer, R. Zameroski, A. Cornelius, T. Schmitz, Freeform Hybrid Manufacturing: Binderjet, Structured Light Scanning, Confocal Microscopy, and CNC Machining, Journal of Manufacturing and Materials Processing 2023, Vol. 7, Page 79. 7 (2023) 79. https://doi.org/10.3390/JMMP7020079.
[22] D. Gilmer, L. Han, E. Hong, D. Siddel, A. Kisliuk, S. Cheng, D. Brunermer, A. Elliott, T. Saito, An in-situ crosslinking binder for binder jet additive manufacturing, Addit Manuf. 35 (2020) 101341. https://doi.org/10.1016/j.addma.2020.101341.
[23] D.B. Gilmer, L. Han, M.L. Lehmann, D.H. Siddel, G. Yang, A.U. Chowdhury, B. Doughty, A.M. Elliott, T. Saito, Additive manufacturing of strong silica sand structures enabled by polyethyleneimine binder, Nat Commun. 12 (2021) 1–8. https://doi.org/10.1038/s41467-021-25463-0.
[24] L. Donati, B. Reggiani, R. Pelaccia, G. Valli, I. Todaro, R. Squatrito, L. Tomesani, T. Pinter, E. Mainetti, Y. Rami, Additive manufacturing of H-13 inserts for optimal extrusion die cooling, n.d.
[25] T. Vu Thang, N. Van Khoi, P. Thi Thu Ha, T. Duc Cong, H. Thi Phuong, N. Van Manh, SYSTHESIS AND CHARACTERIZATION OF POLY (N-VINYL PYRROLIDON-co-VINYL ACETATE), 2014.
[26] K. Sakai, T. Hirano, M. Hosoda, Rapid measurement of ultrahigh viscosity using an electro-magnetically spinning system Related content Electromagnetically Spinning Sphere Viscometer, Japanese Journal of Applied Physics BRIEF NOTE. (2014). https://doi.org/10.7567/JJAP.53.07KC01.
[27] B.P. Jacobs, J.N. Brantley, Exploring Combinatorial Approaches to Polymer Diversification, Macromolecules. 53 (2020) 9287–9293. https://doi.org/10.1021/ACS.MACROMOL.0C01538/SUPPL_FILE/MA0C01538_SI_001.PDF.
[28] A. Friederich, J.R. Binder, W. Bauer, Rheological control of the coffee stain effect for inkjet printing of ceramics, Journal of the American Ceramic Society. (2013). https://doi.org/10.1111/jace.12385.
[29] K.K.B. Hon, L. Li, I.M. Hutchings, Direct writing technology-Advances and developments, CIRP Ann Manuf Technol. 57 (2008) 601–620. https://doi.org/10.1016/j.cirp.2008.09.006.
[30] D. Nichetti, I. Manas-Zloczower, Viscosity model for polydisperse polymer melts, J Rheol (N Y N Y). 42 (1998) 951–969. https://doi.org/10.1122/1.550908.
[31] B.W. R Krigbaum, P.J. Flory, W.G. McMillan, J.E. Mayer, Statistical Mechanics of Dilute Polymer Solutions. IV. Variation of the Osmotic Second Coefficient with Molecular Weightla,h, UTC, 1945. https://pubs.acs.org/sharingguidelines.
[32] B. Derby, Inkjet Printing of Functional and Structural Materials: Fluid Property Requirements, Feature Stability, and Resolution, Annu Rev Mater Res. 40 (2010) 395–414. https://doi.org/10.1146/annurev-matsci-070909-104502.
[33] E.M. Wilts, T.E. Long, Sustainable additive manufacturing: predicting binder jettability of water-soluble, biodegradable and recyclable polymers, Polym Int. 70 (2021) 958–963. https://doi.org/10.1002/pi.6108.

[34] J. Moon, J.E. Grau, V. Knezevic, M.J. Cima, E.M. Sachs, Ink-Jet Printing of Binders for Ceramic Components, Journal of the American Ceramic Society. 85 (2004) 755–762. https://doi.org/10.1111/j.1151-2916.2002.tb00168.x.
[35] N. Reis, B. Derby, Ink Jet Deposition of Ceramic Suspensions: Modeling and Experiments of Droplet Formation, MRS Online Proceedings Library 2000 625:1. 625 (2000) 117–122. https://doi.org/10.1557/PROC-625-117.
[36] N. Reis, C. Ainsley, B. Derby, Viscosity and Acoustic Behavior of Ceramic Suspensions Optimized for Phase-Change Ink-Jet Printing, Journal of the American Ceramic Society. 88 (2005) 802–808. https://doi.org/10.1111/j.1551-2916.2005.00138.x.
[37] J.K. Fink, The Chemistry of Printing Inks and Their Electronics and Medical Applications, 2014. https://doi.org/10.1002/9781119041337.
[38] R.H. Leach, R.J. Pierce, E.P. Hickman, M.J. Mackenzie, H.G. Smith, The Printing Ink Manual, 2007.
[39] B. Utela, D. Storti, R. Anderson, M. Ganter, A review of process development steps for new material systems in three dimensional printing (3DP), J Manuf Process. 10 (2008) 96–104. https://doi.org/10.1016/j.jmapro.2009.03.002.
[40] Y. Bai, C. Wall, H. Pham, A. Esker, C.B. Williams, Characterizing Binder–Powder Interaction in Binder Jetting Additive Manufacturing Via Sessile Drop Goniometry, J Manuf Sci Eng. (2018). https://doi.org/10.1115/1.4041624.
[41] H. Miyanaji, S. Zhang, L. Yang, A new physics-based model for equilibrium saturation determination in binder jetting additive manufacturing process, Int J Mach Tools Manuf. (2018). https://doi.org/10.1016/j.ijmachtools.2017.09.001.
[42] R. Calvert, Applied pyrolysis handbook, 2007. https://doi.org/10.1365/s10337-007-0431-3.
[43] Pyrolysis – Gas Chromatography Mass Spectrometry of, n.d.
[44] P. Das, P. Tiwari, The effect of slow pyrolysis on the conversion of packaging waste plastics (PE and PP) into fuel, Waste Management. 79 (2018) 615–624. https://doi.org/10.1016/j.wasman.2018.08.021.
[45] R.K. Singh, B. Ruj, A.K. Sadhukhan, P. Gupta, A TG-FTIR investigation on the co-pyrolysis of the waste HDPE, PP, PS and PET under high heating conditions, Journal of the Energy Institute. 93 (2020) 1020–1035. https://doi.org/10.1016/j.joei.2019.09.003.
[46] S. Menargues, A. Marcilla, A. Go, TG / FTIR study of the thermal pyrolysis of EVA copolymers, 74 (2005) 224–230. https://doi.org/10.1016/j.jaap.2004.09.009.